ChemComm

COMMUNICATION

View Article Online
View Journal | View Issue

Cite this: *Chem. Commun.*, 2025, **61**, 965

Received 17th September 2024,
Accepted 25th November 2024

DOI: 10.1039/d4cc04820b

rsc.li/chemcomm

Tuning the selectivity of bimetallic Cu electrocatalysts for CO_2 reduction using atomic layer deposition†

Si Young Lee, ‡[a] Julia D. Lenef,‡[b] Daniel O. Delgado Cornejo,[b] Alondra M. Ortiz-Ortiz,[a] Tao Ma,[c] Timothy S. Arthur,[d] Charles A. Roberts *[d] and Neil P. Dasgupta *[ab]

Cu–Zn bimetallic catalysts were synthesized on 3-D gas diffusion electrodes using atomic layer deposition (ALD) techniques. Electrochemical CO_2 reduction was evaluated, and a significant variation in the product selectivity was observed compared to unmodified Cu catalysts. As low as a single ALD cycle of ZnO resulted in a reduction of C_2H_4 production and shift towards CO selectivity, which is attributed to changes in the chemical state of the surface. Our findings demonstrate the impact of atomically-precise surface modifications on electrocatalyst selectivity.

The electrochemical CO_2 reduction reaction (CO_2RR) has garnered significant attention as a promising carbon utilization technology to convert CO_2, a major contributor to the climate crisis, into valuable products using renewable energy sources.[1] In particular, extensive research has been conducted on Cu-based catalysts to produce value-added C_{2+} compounds.[2,3] Owing to the ability of these catalysts to generate more than 16 different products, control of selectivity is a critical issue for the commercialization of CO_2RR technology.[4] Recent studies have shown that enhanced C–C coupling can be achieved by (1) tuning the nanostructure morphology,[5,6] (2) controlling crystal facets or shapes,[7,8] (3) alloying or introducing secondary metals,[9,10] and (4) adjusting the chemical state of the Cu catalyst surface or interfacial environment.[11,12] Such studies indicate that further analysis of catalyst surface modification and interfacial environments is necessary.

Atomic layer deposition (ALD) is a powerful technique that enables programmable control of the surface composition and coating thickness with sub-nm precision.[13] ALD offers an effective method for catalyst deposition by conformally depositing metal nanoparticles (NPs) on porous, high-aspect ratio structures.[14,15] Beyond simple binary oxides, ALD enables the precise control of stoichiometry of solid solutions and alloy materials,[16] which allows for tuning of the chemical state and lattice constants of the catalyst. In addition to synthesis of the catalyst material itself, ALD has also been explored for deposition of saturated, sub-monolayer "overcoats" on catalyst surfaces, which can modulate the adsorption energy of intermediates on the catalyst surface, and also has been shown to improve catalyst stability during operation.[17–20]

Despite these benefits of ALD for precise catalyst synthesis and modification, there have been few reports to date of ALD for Cu-based CO_2RR catalysts.[21] Recently, we reported a plasma-enhanced ALD (PEALD) process to incorporate Cu NP catalysts onto gas diffusion electrodes (GDEs), achieving a high Faradaic efficiency (FE) of over 75% for C_{2+} products.[22] Additionally, ALD of CuS_x electrocatalysts for CO_2RR have been reported to be effective in improving the selectivity of formate.[23] Furthermore, ALD overcoats of metal oxides have been applied to CuO nanowires to tune selectivity.[17,18] This indicates the need for further studies to understand the factors that influence the product selectivity of Cu catalyst architectures using ALD.

In previous studies on Cu-based bimetallic catalysts for CO_2RR using alternative synthetic strategies, elements such as Au, Ag, and Zn have been introduced to modify the selectivity of C_{2+} products such C_2H_4 and C_2H_5OH (EtOH), while Sn has been introduced to improve the selectivity of C_1 products such as formate.[24–26] The introduction of elements such as Ag and Au has been known to improve the selectivity towards EtOH due to the spillover effect of the generated CO,[24,27] but the economic burden of precious metal introduction can be a limiting factor. Recent studies on Cu–Zn bimetallic catalysts have shown inconsistent trends in selectivity, with either C_1 or C_2 products increasing depending on the method and ratio of Zn introduction.[25,28–30] However, there have been no reports to date of bimetallic Cu-based NP catalysts deposited by ALD.

In this study, we expand up on our previously developed PEALD method for Cu catalysts,[22,31] and explore the deposition of Cu–Zn bimetallic alloys and Cu@ZnO core–shell catalysts with a ZnO overcoat

[a] *Department of Mechanical Engineering, University of Michigan, Ann Arbor, MI 48109, USA. E-mail: ndasupt@umich.edu*
[b] *Department of Materials Science & Engineering, University of Michigan, Ann Arbor, MI 48109, USA*
[c] *Michigan Center for Materials Characterization, University of Michigan, Ann Arbor, MI 48109, USA*
[d] *Toyota Research Institute of North America, Ann Arbor, MI, 48105, USA. E-mail: charles.roberts@toyota.com*

† Electronic supplementary information (ESI) available: Experimental section, SEM, images, XRD, XPS data and electrochemical results. See DOI: https://doi.org/10.1039/d4cc04820b

‡ These authors contributed equally to this work.

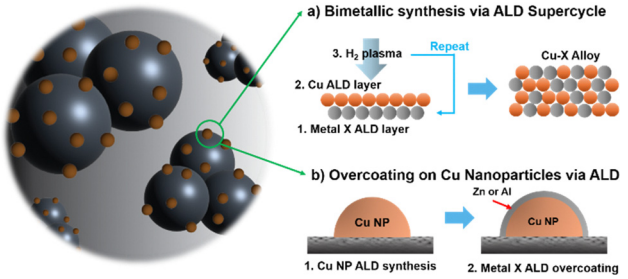

Scheme 1 Cu bimetallic catalyst synthesis strategy that can be introduced through ALD.

on Cu (Scheme 1). Using these two model systems, we measured the effects of Zn introduction on product selectivity. The influences of these chemical and structural changes on the Cu catalyst are described below.

To fabricate Cu–Zn bimetallic alloy NPs, a supercycle approach was used alternating ALD Cu and ZnO cycles in a 9 : 1 ratio (Scheme 1a). This is a common strategy to generate multi-element ALD films, where both elements are incorporated into the bulk material.[32] Experimental details on the ALD process are provided in the ESI.†

Scanning electron microscopy (SEM) and scanning transmission electron microscopy (STEM) were performed to examine the morphology of the catalyst surfaces on carbon GDE substrates. Fig. 1a and Fig. S1 (ESI†) shows an SEM and TEM image of Cu NPs (4 ± 1 nm) after depositing 510 PEALD Cu cycles. The bimetallic alloy NPs had a slightly larger diameter 9 ± 2 nm, while maintaining a uniform distribution across the complex 3-D GDE structure (Fig. 1b and Fig. S2, ESI†). We have previously shown that varying the ALD Cu NP size in the nanometer range had a minimal effect on product selectivity, so these slight differences in particle diameter are not expected to have a strong effect. In both instances, the ability to conformally distribute NPs on a high aspect-ratio 3-D substrate demonstrates the power of the ALD method for electrocatalyst architectures.

The supercycle approach resulted in an approximately 1 : 1 ratio of Cu : Zn, as confirmed using X-ray photoelectron spectroscopy (XPS) (Table S1, ESI†). Further evidence of the formation of a bimetallic alloy was observed by STEM-energy dispersive X-ray spectroscopy (EDS) mapping (Fig. S3, ESI†) and the change in visible color, which appeared similar to brass (Fig. S4, ESI†). Grazing incidence X-ray diffraction (XRD) analysis revealed that the 2-theta value of (002) shifted to a lower angle by 0.96 degrees when Zn was introduced to the Cu catalyst, indicating an increase in *d*-spacing (Fig. 1c). This can be rationalized by the fact that Zn has a larger atomic radius than Cu.

The presence of Zn in the Cu catalyst significantly impacted overall product selectivity. Chronoamperometry measurements were performed for each system (Cu and Cu–Zn) at a potential of −0.93 V and −0.90 V *vs.* RHE, respectively, for 1 hour. The gas-phase products were quantified using gas chromatography. The pure Cu metal sample exhibited a ∼38% FE for C_2H_4 (Fig. 1d) which is consistent with the previously report.[21] In contrast, the Cu–Zn bimetallic catalyst reduced this value to below 3%, and the CO content increased by about 31%. This represents an order-of-magnitude change in the selectivity for each of these products, illustrating the strong impact of Zn on the selectivity.

To examine the influence of Zn alloying on the chemical environment of Cu, XPS core scans were collected at the Cu 2p peak position. The presence of Zn resulted in a shift to lower binding energies for the Cu atoms (Cu PEALD: 933.3 eV, CuZn: 932.9 eV), indicating a shift to a more electron-rich environment (Fig. 1e).[33] This shift is attributed to the lower electronegativity of the Zn atom compared to Cu. This result suggests that an electron-rich Cu state might be favorable for CO production.

To study the influence of the Zn concentration in the alloy on the chemical structure and corresponding product selectivity, bimetallic catalysts with a lower Zn content were synthesized. To accomplish this, the ALD cycle ratio of Cu : Zn in the supercycle recipe was increased from 9 : 1 to 81 : 1. XPS analysis showed a surface atomic ratio of about 3 : 1 (Table S1, ESI†).

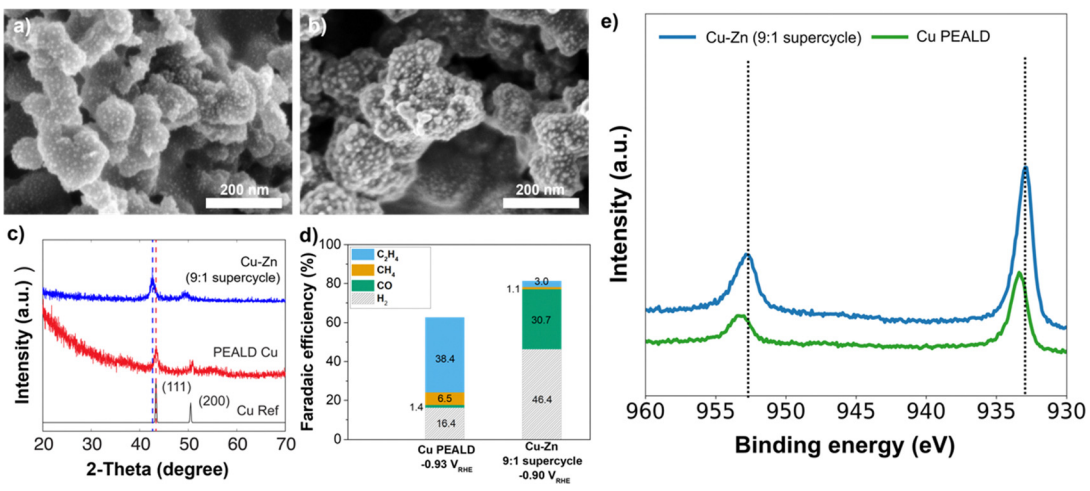

Fig. 1 (a) SEM image of Cu PEALD catalyst on carbon GDE support. (b) SEM image of Cu–Zn (9 : 1 supercycle) bimetallic catalyst on GDE support. (c) XRD spectrum of Cu PEALD and Cu–Zn (9 : 1 supercycle) bimetallic catalyst on Si substrate (ICDS no: 15985). (d) Comparison of the Faradaic efficiency of the gaseous products for the Cu catalyst at −0.93 V *vs.* RHE and the Cu–Zn (9 : 1 supercycle) bimetallic catalyst at −0.90 V *vs.* RHE. (e) Cu 2p XPS spectra of Cu and Cu–Zn (9 : 1 supercycle) bimetallic catalysts on GDE substrate after 1 min Ar sputtering.

Examining a simple rule-of-mixtures analysis, these trends in stoichiometry suggest a nucleation delay of Cu growth on ZnO (Fig. S5, ESI†). The 81 : 1 supercycle catalyst had similar NP sizes to pure Cu PEALD (Fig. S6a, ESI†). In contrast to the 9 : 1 supercycle catalyst, which produces 30.7% CO at −0.90 V *vs.* RHE, the 81 : 1 supercycle catalyst with a lower Zn ratio suppresses CO production to around 10% FE across a wider potential range. The 81 : 1 supercycle sample also exhibits one order-of-magnitude lower FE for CH_4 at potentials more negative than −0.90 V *vs.* RHE (Fig. S6b and c, ESI†), showing a higher suppression of C_1 products compared to the 9 : 1 catalyst. These results suggest that in Cu–Zn bimetallic catalysts synthesized by ALD methods, reducing the amount of Zn introduced can enhance the total activity and C–C coupling selectivity of the catalyst. Further analysis and discussion of the 81 : 1 supercycle catalysts is provided in the ESI.†

To study the influence of how the Zn atoms were incorporated into the Cu NP catalysts during the ALD process, an overcoating strategy was also explored to form a core–shell structure, rather than mixing Zn into the bulk of the NP (Scheme 1b). For these samples, a series of ALD ZnO depositions were performed using 1, and 3 cycles on the surface of PEALD Cu catalysts. While the alloying method resulted in slight variations in NP morphology and size according to Cu–Zn ratios, the NP size and morphology remained similar across different cycles of ZnO ALD on Cu (Fig. 2a and Fig. S8, ESI†). This further illustrates the core–shell effect, as 1–3 cycles of ALD ZnO corresponds to only around 2–6 anstroms of nominal thickness. In other words, the NP nucleation and growth is determined by the PEALD Cu process, while the ALD ZnO overcoat conformally coats the NP topology.

Fig. 2b displays the product analysis for the Cu PEALD and 1–3 ALD overcoat cycles on PEALD Cu catalysts. Notably, the selectivity for C_2H_4 drastically decreased to 9.8% at −0.95 V *vs.* RHE after only 1 cycle of ZnO ALD, compared to nearly 38.4% at −0.93 V *vs.* RHE for pristine Cu PEALD. Furthermore, the selectivity towards CO increased over an order of magnitude. This indicates that even minimal Zn introduction (a nominal overcoat thickness of ∼2 angstroms, which corresponds to less than a single unit cell of crystalline ZnO) can significantly alter catalyst selectivity. After additional ALD depositions of 3 cycles, the C_2H_4 selectivity dropped further to 4.2% at −0.93 V *vs.* RHE, with a slight increase in CO production (from 20.7% to 22.5%), These trends in FE were similar at various potentials for each catalyst (Fig. S9, ESI†), and the current density (activity) was also similar under each condition (Fig. S10, ESI†). This illustrates that the first ALD cycle of ZnO had the most profound effect on selectivity, while further increases in the surface Zn concentration had less significant effects.

The Cu 2p binding energy measured by XPS for pure Cu catalysts was 933.3 eV, and the Cu with a 1-cycle ZnO overcoat (CZ1) catalyst shows a nearly identical value at 933.2 eV (Fig. 2c). When a ZnO ALD overcoat is applied using 3 cycles, the Cu 2p binding energy shifts to 932.9 eV, similar to that of the CuZn alloy catalyst, and the FE also changes accordingly. This indicates that the surface properties and the chemical state of Cu can change significantly within a ZnO layer thickness range of around 2–6 angstroms. These findings suggest that in Cu–Zn systems, not only does the chemical state of Cu change due to the interaction between Cu and Zn, but even a few angstrom-thick hetero-structure ALD layer on the catalyst surface can significantly impact CO_2RR performance (*i.e.*, CO_2 adsorption, intermediate surface diffusion, *etc.*).

To examine whether other metal oxide overcoats would also result in these significant shifts in CO_2RR selectivity, another sample was fabricated coating Cu PEALD catalysts with 1 cycle of Al_2O_3 (CA1). SEM imaging of this catalyst showed a similar morphology to the pristine Cu PEALD catalysts (Fig. S11, ESI†). Unlike the CZ1 sample, which predominantly produced 9.8% C_2H_4 and 20.7% CO at −0.95 V *vs.* RHE, the CA1 sample had a similar C_2H_4 FE of 32.7% to Cu PEALD at −0.91 V *vs.* RHE (Fig. 3a). This tendency in CA1 remained similar across other potential ranges (Fig. S12, ESI†). Despite the 1 : 4 Cu : Al ratio revealed by XPS analysis (Table S2, ESI†), the CA1 catalyst exhibited similar C_2H_4 selectivity to that of pure Cu, implying different impacts on Cu selectivity depending on the metallic element used in the overcoat.

To study the influence of the Al_2O_3 and ZnO overcoats on the surface binding environment, Cu 2p XPS core scans were measured without any Ar sputtering (Fig. 3b). The trend in observed binding energies was Cu (933.3 eV) > CZ1 (933.2 eV) > CA1 (932.9 eV). After Ar sputtering, all three samples showed the same binding energy (Fig. S14, ESI†). This indicates that the impacts of single-cycle ALD overcoats on the Cu chemical state is highly localized to the surface.

We also observe a difference in the satellite peak near 944 eV, which is associated with the Cu^{2+} oxidation state.[11,33] The ALD ZnO process

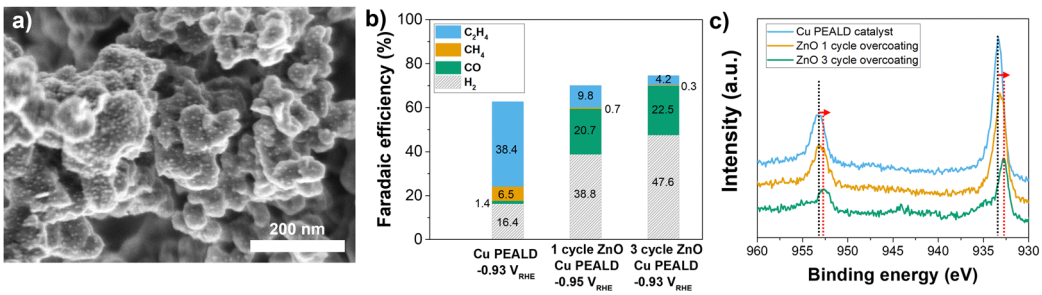

Fig. 2 (a) SEM image after 1 cycle ZnO ALD overcoating on a bare Cu PEALD catalyst. (b) FE comparison of gaseous products of the catalyst Cu PEALD and after 1, and 3 cycles of ZnO ALD overcoats. (c) Comparison of Cu 2p XPS spectra of Cu PEALD catalyst and after 1, and 3 cycle ZnO ALD overcoating after 1 min Ar sputtering treatment.

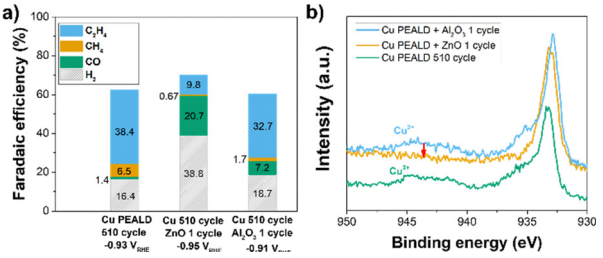

Fig. 3 (a) FE of gaseous products using a pristine Cu PEALD catalyst, 1 cycle ZnO ALD overcoat, and 1 cycle Al_2O_3 ALD overcoat. (b) Comparison of Cu 2p XPS spectra of each catalyst sample with no Ar sputtering used in the measurement.

reduces the presence of Cu^{2+} species on the Cu NP surface, unlike the ALD Al_2O_3 process, which preserved the Cu^{2+} surface oxide layer. Previous studies on copper oxide-based CO_2RR catalysts indicated that reduction of Cu oxide layers could enhance C_2H_4 selectivity,[11,34–36] which suggests that the ability to maintain surface oxides might contribute to the differences in C_2H_4 selectivity. These results suggest that ALD overcoating strategies for CO_2RR catalysts must consider not only the composition of the coating material, but also changes in the surface oxidation of the underlying substrate.

To investigate the role of the Al_2O_3 overcoat on the electrocatalyst stability, chronoamperometry tests were conducted on the CA1 catalyst (Fig. S13, ESI†). The CA1 catalyst maintained a stable current density of ~ -28 mA cm^{-2} at -0.93 V *vs.* RHE for 24 hours. However, the FE for C_2H_4 increased from 28.5% to 35.2% in the first 3 hours before decreasing, while H_2 selectivity increased continuously. This differs from previous observations where Cu PEALD showed a more monotonic trend in stability.[22] These results suggest that ALD overcoats can also influence the surface reconstruction processes of Cu catalysts under CO_2RR conditions, necessitating further research.

In conclusion, Zn was introduced into PEALD Cu NP catalysts using both alloying and overcoating methods. It was proposed that the electron-rich environment of Cu atoms induced by Zn may contribute to decreased C–C coupling selectivity. Additionally, ultrathin ALD overcoats altered the chemical state of Cu and consequently reduced the C_2H_4 selectivity. By changing the overcoat material from ZnO to Al_2O_3, the selectivity for C_2 products remained similar to that of Cu. These differences suggest that altering the surface chemistry of Cu with overcoats can have a profound impact on selectivity. Overall, this work highlights the power of ALD to both tune and understand the mechanisms that determine CO_2RR selectivity.

This research was supported by Toyota Research Institute of North America (TRINA) and by the National Science Foundation under Grant No. 2131709.

Data availability

The data supporting this article have been included as part of the ESI.†

Conflicts of interest

There are no conflicts to declare.

Notes and references

1 O. S. Bushuyev, P. D. Luna, C. T. Dinh, L. Tao, G. Saur, J. V. D. Lagemaat, S. O. Kelley and E. H. Sargent, *Joule*, 2018, **2**, 825–832.
2 M. Jiang, H. Wang, M. Zhu, X. Luo, Y. He, M. Wang, C. Wu, L. Zhang, X. Liao, Z. Jiang and Z. Jin, *Chem. Soc. Rev.*, 2024, **53**, 5149–5189.
3 P. D. Luna, C. Hahn, D. Higgins, S. A. Jaffer, T. F. Jaramillo and E. H. Sargent, *Science*, 2019, **364**, 350.
4 K. P. Kuhl, E. R. Cave, D. N. Abram and T. F. Jaramillo, *Energy Environ. Sci.*, 2012, **5**, 7050–7059.
5 K. D. Yang, W. R. Ko, J. H. Lee, S. J. Kim, H. Lee, M. H. Lee and K. T. Nam, *Angew. Chem., Int. Ed.*, 2017, **56**, 796–800.
6 M. Jun, C. Kwak, S. Y. Lee, J. Joo, J. M. Kim, D. J. Im, M. K. Cho, H. Baik, Y. J. Hwang, H. Kim and K. Lee, *Small Methods*, 2022, **6**, 2200074.
7 G. L. D. Gregorio, T. Burdyny, A. Loiudice, P. Iyengar, W. A. Smith and R. Buonsanti, *ACS Catal.*, 2020, **10**, 4854–4862.
8 J. A. Gauthier, J. H. Stenlid, F. Abild-Pedersen, M. Head-Gordon and A. T. Bell, *ACS Energy Lett.*, 2021, **6**, 3252–3260.
9 K. Tran and Z. W. Ulissi, *Nat. Catal.*, 2018, **1**, 696–703.
10 L. Xie, J. Liang, C. Priest, T. Wang, D. Ding, G. Wu and Q. Li, *Chem. Commun.*, 2021, **57**, 1839–1854.
11 S. Y. Lee, H. Jung, N.-K. Kim, H.-S. Oh, B. K. Min and Y. J. Hwang, *J. Am. Chem. Soc.*, 2018, **140**, 8681–8689.
12 S. Y. Lee, J. Kim, G. Bak, E. Lee, D. Kim, S. Yoo, J. Kim, H. Yun and Y. J. Hwang, *J. Am. Chem. Soc.*, 2023, **145**, 23068–23075.
13 S. M. George, *Chem. Rev.*, 2010, **110**, 111–131.
14 B. J. O'Neil, D. H. K. Jackson, J. Lee, C. Canlas, P. C. Stair, C. L. Marshall, J. W. Elam, T. F. Kuech, J. A. Dumesic and G. W. Huber, *ACS Catal.*, 2015, **5**, 1804–1825.
15 C. Detavernier, J. Dendooven, S. P. Sree, K. F. Ludwig and J. A. Matens, *Chem. Soc. Rev.*, 2011, **40**, 5242–5253.
16 J. Lu, K.-B. Low, Y. Lei, J. A. Libera, A. Nicholls, P. C. Stair and J. W. Elam, *Nat. Commun.*, 2014, **5**, 3264.
17 M. Schreier, F. Héroguel, L. Steier, S. Ahmad, J. S. Luterbacher, M. T. Mayer, J. Luo and M. Grätzel, *Nat. Energy*, 2017, **2**, 17087.
18 D. Ren, J. Gao, L. Pan, Z. Wang, J. Luo, S. M. Zakeeruddin, A. Hagfeldt and M. Grätzel, *Angew. Chem., Int. Ed.*, 2019, **58**, 15036–15040.
19 J. Lu, B. Fu, M. C. Kung, G. Xiao, J. W. Elam, H. H. Kung and P. C. Stair, *Science*, 2012, **335**, 1205–1208.
20 N. Cheng, M. N. Banis, J. Liu, A. Riese, X. Li, R. Li, S. Ye, S. Knights and X. Sun, *Adv. Mater.*, 2015, **27**, 277–281.
21 J. O. Olowoyo, V. S. Gharahshiran, Y. Zeng and Y. Zheng, *Chem. Soc. Rev.*, 2024, **53**, 5428–5488.
22 J. D. Lenef, S. Y. Lee, K. M. Fuelling, K. E. Rivera Cruz, A. Prajapati, D. O. Delgado Cornejo, T. H. Cho, K. Sun, E. Alvarado, T. S. Arthur, C. A. Roberts, C. Hahn, C. C. L. McCrory and N. P. Dasgupta, *Nano Lett.*, 2023, **23**, 10779–10787.
23 M. Suominen, M. Mäntymäki, M. Mattinen, J. Sainio, M. Putkonen and T. Kallio, *Mater. Today Sustainability*, 2023, **24**, 100575.
24 Y. Lum and J. W. Ager, *Energy Environ. Sci.*, 2018, **11**, 2935–2944.
25 J. Zhang, C. Guo, S. Fang, X. Zhao, L. Li, H. Jiang, Z. Liu, Z. Fan, W. Xu, J. Xiao and M. Zhong, *Nat. Commun.*, 2023, **14**, 1298.
26 M. Zhang, Z. Zhang, Z. Zhao, H. Huang, D. H. Anjum, D. Wang, J.-H. He and K.-W. Huang, *ACS Catal.*, 2021, **11**, 11103–11108.
27 E. L. Clark, C. Hahn, T. F. Jaramillo and A. T. Bell, *J. Am. Chem. Soc.*, 2017, **139**, 15848–15857.
28 Y. Feng, Z. Li, H. Liu, C. Dong, J. Wang, S. A. Kulinich and X. Du, *Langmuir*, 2018, **34**, 13544–13549.
29 H. S. Jeon, J. Timoshenko, F. Scholten, I. Sinev, A. Herzog, F. T. Haase and B. R. Cuenya, *J. Am. Chem. Soc.*, 2019, **141**, 19879–19887.
30 L. Wan, X. Zhang, J. Cheng, R. Chen, L. Wu, J. Shi and J. Luo, *ACS Catal.*, 2022, **12**, 2741–2748.
31 J. D. Lenef, J. Jo, O. Trejo, D. J. Mandia, R. L. Peterson and N. P. Dasgupta, *J. Phys. Chem. C*, 2021, **125**, 9383–9390.
32 A. R. Bielinski, S. Lee, J. J. Brancho, S. L. Esarey, A. J. Gayle, E. Kazyak, K. Sun, B. M. Bartlett and N. P. Dasgupta, *Chem. Mater.*, 2019, **31**, 3221–3227.
33 J. Conradie and E. Erasmus, *J. Electron. Spectrosc. Relat. Phenom.*, 2022, **259**, 147241.
34 S. Y. Lee, S. Y. Chae, H. Jung, C. W. Lee, D. L. T. Nguyen, H.-S. Oh, B. K. Min and Y. J. Hwang, *J. Mater. Chem. A*, 2020, **8**, 6210–6218.
35 R. M. Arán-Ais, F. Scholten, S. Kunze, R. Rizo and B. R. Cuenya, *Nat. Energy*, 2020, **5**, 317–325.
36 X. Li, L. Li, L. Wang, Q. Xia, L. Hao, X. Zhan, A. W. Robertson and Z. Sun, *Chem. Commun.*, 2022, **58**, 7412–7415.